Supplementary Experimental Procedures

Analysis of the oligomeric state of S1C mutants

Since SOAR fragments (Figure S1iA) have been shown to form dimers (Covington et al., 2010; Maus et al., 2015; Muik et al., 2011; Yang et al., 2012; Yuan et al., 2009; Zhou et al., 2013, 2015) and tetramers (Park et al., 2009) we initially considered the possibility that changes in the oligomeric state of the SOAR mutants may establish the basis for the physical and functional interaction pattern between S1C mutants and Orai1 or Orai1-S channels.
To study the oligomeric state of each of the S1C mutants we expressed EGFP-tagged S1C in HEK293 cells and employed a single-molecule pull-down (SiMPull) assay to isolate protein from cell lysate, display at low density on a passivated coverslip (Figure S1iB) and determine their subunit stoichiometry using single molecule photo-bleaching in total internal reflection microscopy (Jain et al., 2012). As shown in Figure S1iC, the majority of the EGFP molecules attached to S1C construct bleached in two steps indicating dimeric assembly of S1C subunits. Furthermore and consistent with dimeric assembly of S1C proteins, the majority of EGFP molecules bleached in a single step when EGFP is attached to an S domain concatemer–dimer construct (Figure S1iD). Most EGFP molecules attached to S1C F394H construct bleached in two steps indicating similar dimeric organization as wt S1C (Figure S1iE). EGFP molecules attached to S1C 4KA or to S1C R429C constructs bleached in either one or two steps evenly (Figure S1iE), suggesting that these S1C mutants may be slightly deficient in forming dimers or that the fused GFP molecules suffer from reduced protein maturation. To further explore the oligomeric state of S1C mutants and to investigate their ability to form hetero-dimers with wt subunits we studied the number of EGFP photobleaching events recorded when EGFP-S1C was expressed together with wt or mutant S1C constructs tagged with mCherry. Given the distinct spectral properties of EGFP and mCherry, the rationale behind this experiment is that co-assembly of EGFP-S1C subunits with mCherry-S1C subunits would shift the observed distribution of S1C molecules with two photobleaching events to lower values (Figure S1iF). When wt or mutant mCherry-S1C constructs were co-expressed with EGFP-S1C we observed a substantial increase in the frequency of single EGFP photobleaching events (indicative of "silent" mCherry tag at the expense of EGFP tag) compared to their frequency when EGFP-S1C constructs are expressed alone (Figure S1iE). This effect was slightly smaller for mCherry-S1C 4KA or R429C constructs compared to wt, consistent with only a slight reduction in the ability of these S1C mutants to form dimers with the wt fragment.

Taken together and consistent with earlier studies (Covington et al., 2010; Maus et al., 2015; Muik et al., 2011; Yang et al., 2012; Yuan et al., 2009; Zhou et al., 2013, 2015), these results indicate that all mutant S1C constructs exists mostly as dimers and are able to form hetero-dimers with wt subunits.

Analysis of the 4KA SOAR mutant

While in the majority of cells co-expressing S1C 4KA together with Orai1 no current was recorded, in 4 out of 18 cells normal CRCA like current was developed. This current grow slowly than in cells expressing wt S1C but when stabilized it displayed similar density and current-voltage relation as wt S1C (Figures S1IID-E). This finding was also verified by analyzing nuclear translocation of NFAT (Figure S1iiB). The deficiency of the 4KA mutant can be overcome by increasing in the expression level of SOAR 4KA constructs. Western blot analysis shown in Figure SIIA indicates that concatenated dimer constructs of SOAR (SS-EGFP) are expressed at higher levels than monomeric SOAR constructs (EGFP-S1C). However, while expression of both wt and mutant SS-EGFP constructs is increased compared to the corresponding EGFP-S1C constructs, currents are augmented only in cells co-expressing the 4KA mutant together with Orai1 suggesting that increasing the concentration of the 4KA mutant, but not the F394H or R429C mutants, can rescue channel activation. The relationship between EGFP-S1C 4KA expression levels and Orai1 activation was further assessed by analyzing the cellular localization of NFAT as a function of protein expression, as judged by EGFP fluorescence. Expression levels of S1C 4KA in cells exhibiting nuclear localization of NFAT were higher than in cells with cytosolic localization of NFAT, but this difference did not reach statistical significance (Figure S1iiC). Lastly, as a third approach to address if the 4KA mutant activates Orai1 channels in a concentration dependent manner we increased the local concentration of SOAR around Orai1 by expressing concatenated Orai1-SOAR constructs with two S domains directly linked to each Orai1 subunit (Orai1-SS). The deficiency of SOAR 4KA in activating Orai1 channels was fully rescued in Orai1-SS 4KA but not in Orai1-SS F394H or R429C (Figure S1iiG) indicating that the weak reactivity of the SOAR 4KA mutant with Orai1 is fully compensated by increasing its local concentration near the channel. Taken together, these results indicate

that the weak capacity of SOAR 4KA for activating Orai1 channels arises at least partially from low affinity of the mutant SOAR to Orai1.

SiMPull Assay

SiMPull was performed on lysates prepared from HEK293 cells transfected with EGFP-tagged S1C constructs as previously described (Bharill et al., 2014). Briefly, channels/flow chambers were prepared on coverslips passivated with monofunctional and with biotinylated polyethylene glycol. Biotinylated anti-EGFP antibody (Abcam) was then immobilized by incubating 40 nM of antibody on Neutravidin (Thermofisher)- pre-coated channels. Sample lysate was flowed through the channels just before imaging by Total Internal Reflection Fluorescence Microscopy (TIRFM). mEGFP-tagged S1C proteins were excited using a phoxX 488 (60 mW) laser and a 495-nm long-pass dichroic mirror was used in combination with a 525/50-nm band-pass filter for emission. Six hundred frames were acquired at 10 Hz using an electronmultiplying charge-coupled device (Andor iXon DV-897 BV) and only single, diffraction-limited spots were analyzed. Individual experiments were repeated twice and about 200 to 800 spots from 5–15 different regions were analyzed per EGFP-S1C or SS-EGFP constructs.

Generation of plasmids

The STIM1-EGFP, Orai1-EGFP, FLAG-mCherry-Orai1 and S1C (fragment corresponding to residues 342-465 of hSTIM1) constructs were previously described (Palty et al., 2012, 2015). The Orai1-HA construct was obtained from Prof. Shmuel Muallem lab at the National Institutes of Health (NIH, USA). The Orai1-S-EGFP and Orai1-SS-EGFP constructs were obtained from Prof. Tao Xu lab at the Chinese Academy of Sciences (Beijing, China). The coding region of Orai1 was removed and from Orai1-SS-EGFP and a new start codon was inserted to generate SS-EGFP. To make O1C-EGFP, a fragment coding for the C terminal region of Orai1 (residues 264-301) was sub-cloned into EGFP-N1. To make FLAG-mCherry-O1N, a fragment coding for the N terminal region of Orai1 was sub-cloned into FLAG-mCherry-Orai1 instead of the full length Orai1 coding region. SNAP-Orai1 and Orai1-SNAP were created by replacing the coding region for mCherry or EGFP with that of SNAP in FLAG-mCherry-Orai1 or Orai1-EGFP constructs, respectively. All point mutations were created by standard site-directed mutagenesis PCR and all plasmids were sent to the DNA Sequencing Facility at UC Berkeley for verification of the modified plasmid regions.

NFAT translocation assay

Cells co-expressing the indicated constructs together with NFAT-mCherry or NFAT-GFP were plated and cultured as described above. At the start of each experiment, cells were washed twice with Ringer's solution containing 2mM Ca^{2+} and kept in the same solution for 45 min after which mid-planes sections of transfected cells were acquired using LSM 780 confocal microscope (Zeiss). Images were analyzed using Image-J to determine cytosolic or nuclear localization of NFAT-mCherry in individual cells. Experiments were repeated two to four times. All data are shown as average ± SEM.

Immunoblot and Immunoprecipitation

Immunoblot and Immunoprecipitation were performed as previously described (Palty et al., 2012)and according to the manufacturers protocols. For additional details see Supplemental Materials and Methods.
24-30 hours after transfection HEK293-T cells were washed twice with PBS solution and placed into lysis buffer (150 NaCl, 10mM TriCl (pH 7.6), 0.5mM EDTA, 0.5% NP-40) containing protease inhibitors (Roche) on ice for 30 min. Samples were homogenized by pipetting and centrifuged for 10 min to dispose cell debris and nuclei. Immunoprecipitation was performed using agarose conjugated Anti-GFP beads (MBL) or Anti-RFP beads (Chromotek, RFP-Trap) according to manufacturer protocol. Proteins were resolved by SDS-PAGE and transferred onto nitrocellulose membranes. The membranes were first blocked with 5% non-fat dry milk in TBS (50 mM Tris, 150 mM NaCl, pH 7.4) for one hour at room temperature, then incubated with one of the primary antibodies diluted in 1% milk-TBS overnight at 4°C, targeted against GFP (MBL, 1:2000 or Abcam 1:5000), FLAG tag (Genscript, 1:2000), Orai1 (Santa-Cruz 1:1000) or Actin (Thermo Fisher, 1:5000), mcherry (Abcam 1:2000). Afterwards the membranes were incubated with appropriate secondary antibodies and protein levels were detected using the enhanced chemiluminescent detection system (Pierce). For re-blotting with another primary antibody, the membranes were washed with stripping buffer (62.5 mM Tris, 2%SDS and 1% 2-Mercaptoethanol) at 50°C for 30

min, then undergo the same blocking and antibody incubation. All Immunoprecipitation and immunoblot experiments were repeated at least twice. Cropped regions of immunoblot membrane scans are displayed in main figures and full image scans are displayed in supplemental figures.

Acceptor Photobleaching and ratiometirc FRET

Cells were labelled using normal culture media supplemented with 0.75 μM BG-TMR (SNAP-Cell TMR-Star, NEB) and 8 μM BG-Oregon-Green (SNAP-Cell Oregon Green, NEB) at 37 °C for 20 minutes and washed with fresh media for additional 20 minutes. Estimation of FRET efficiency by recovery of donor fluorescence after acceptor photobleaching was performed as previously described(Palty et al., 2015). Briefly, cells were imaged in PBS on an LSM 780 confocal microscope (Zeiss). The donor (Oregon Green) was excited at 488 nm and emission collected from 493 to 524 nm, and the acceptor (TMR) was excited at 561 nm and emission collected from 583 to 685 nm. Donor fluorescence was imaged before and after bleaching a region of interest of TMR fluorescence. Following bleaching, TMR fluorescence was decreased to <10% of its initial intensity. FRET energy transfer (FRET efficiency) was calculated as % (FRET efficiency) =100 × (Dpost − Dpre)/Dpost, where Dpre and Dpost are the donor (BG-Oregon Green) intensities before and after acceptor (BG-TMR) bleaching, respectively.
For ratiometric FRET measurements, following BG dye loading coverslips were transferred onto an imaging chamber with extracellular Ringer's solution, mounted on an upright, scanning confocal microscope (Zeiss LSM 780) and imaged with a ×20 objective. Donor excitation was performed using a 561-nm laser and images were acquired in the donor and acceptor channels at 1 Hz. Groups of cells (n=9-21) in each independent experiment) were analyzed together and FRET was calculated as FRET = (IA)/(ID + IA), in which ID is the fluorescence donor intensity, and IA is the fluorescence acceptor intensity. Extracellular solution exchange was performed using a gravity-driven perfusion system.

Supplementary References:

Covington, E.D., Wu, M.M., and Lewis, R.S. (2010). Essential role for the CRAC activation domain in store-dependent oligomerization of STIM1. Mol. Biol. Cell *21*, 1897–1907.

Jain, A., Liu, R., Xiang, Y.K., and Ha, T. (2012). Single-molecule pull-down for studying protein interactions. Nat. Protoc. *7*, 445–452.

Maus, M., Jairaman, A., Stathopulos, P.B., Muik, M., Fahrner, M., Weidinger, C., Benson, M., Fuchs, S., Ehl, S., Romanin, C., et al. (2015). Missense mutation in immunodeficient patients shows the multifunctional roles of coiled-coil domain 3 (CC3) in STIM1 activation. Proc. Natl. Acad. Sci. U. S. A. *112*, 6206–6211.

Muik, M., Fahrner, M., Schindl, R., Stathopulos, P., Frischauf, I., Derler, I., Plenk, P., Lackner, B., Groschner, K., Ikura, M., et al. (2011). STIM1 couples to ORAI1 via an intramolecular transition into an extended conformation. EMBO J. *30*, 1678–1689.

Park, C.Y., Hoover, P.J., Mullins, F.M., Bachhawat, P., Covington, E.D., Raunser, S., Walz, T., Garcia, K.C., Dolmetsch, R.E., and Lewis, R.S. (2009). STIM1 Clusters and Activates CRAC Channels via Direct Binding of a Cytosolic Domain to Orai1. Cell *136*, 876–890.

Yang, X., Jin, H., Cai, X., Li, S., and Shen, Y. (2012). Structural and mechanistic insights into the activation of Stromal interaction molecule 1 (STIM1). Proc. Natl. Acad. Sci. *109*, 5657–5662.

Yuan, J.P., Zeng, W., Dorwart, M.R., Choi, Y.-J., Worley, P.F., and Muallem, S. (2009). SOAR and the polybasic STIM1 domains gate and regulate Orai channels. Nat. Cell Biol. *11*, 337–343.

Zhou, Y., Srinivasan, P., Razavi, S., Seymour, S., Meraner, P., Gudlur, A., Stathopulos, P.B., Ikura, M., Rao, A., and Hogan, P.G. (2013). Initial activation of STIM1, the regulator of store-operated calcium entry. Nat Struct Mol Biol *20*, 973–981.

Zhou, Y., Wang, X., Wang, X., Loktionova, N.A., Cai, X., Nwokonko, R.M., Vrana, E., Wang, Y., Rothberg, B.S., and Gill, D.L. (2015). STIM1 dimers undergo unimolecular coupling to activate Orai1 channels. Nat. Commun. *6*, 8395.

Supplementary Figures and Legends:

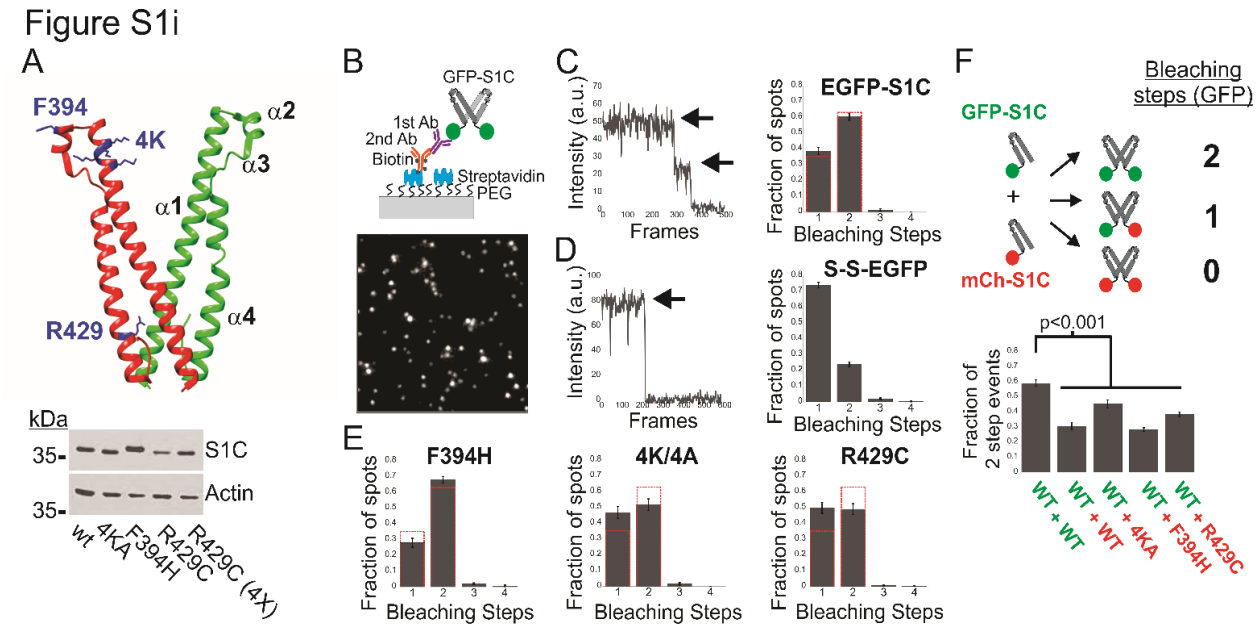

Figure S1i: SOAR mutants 4KA, F394H and R429C form dimers, Related to Figure 1. (A) (Top) Ribbon representation of the crystal structure of the hSOAR dimer (PDB ID:3TEQ). Each SOAR monomer is colored (red and green), helices α1 to α4 are marked and the α1 lysine, α2 F394 and α4 R429 residues mutated in this work are colored in blue. (Lower panel) Western blot analysis of cell lysate prepared from cells expressing the indicated EGFP-S1C constructs. Anti-GFP and anti-Actin antibodies were used for protein detection. Note that R429C EGFP-S1C show comparable expression levels to other S1C constructs when the concentration of EGFP-S1C R429C plasmid used for transfection was increased by four fold (4X). (B) Schematic diagram of single molecule pull-down set-up. Glass surface is passivated with a mix of polyethylene glycol (PEG) and biotinylated PEG. Streptavidin bridges biotinylated PEG and biotinylated secondary antibody. Secondary antibody binds to primary antibody to immobilize the EGFP tagged S1C protein complex to the glass surface. Image shows a representative single frame from a movie of a glass surface following EGFP-S1C pull-down. (C) Representative trace showing the time course of fluorophore photobleaching of an individual spot of EGFP-S1C. Arrows signify a two-step photobleaching event (left). The average frequency distributions of the number of bleaching steps from individual experiments (right). (D) Representative photobleaching trace of an individual spot of SS-EGFP showing one-step photobleaching event (left). The average frequency distributions of the number of bleaching steps from individual experiments (right). (E) Single-molecule counting of GFP bleaching steps per fluorescent spot for the indicated EGFP-S1C mutants. (F) Schematic illustration of three types of dimers formed by mCherry or EGFP tagged S1C proteins and their expected number of GFP bleaching steps (Left). The average frequency of two bleaching steps from individual experiments (right). Dashed red line indicates theoretical binominal distribution for a dimer with EGFP fluorescence maturation probability = 0.80.

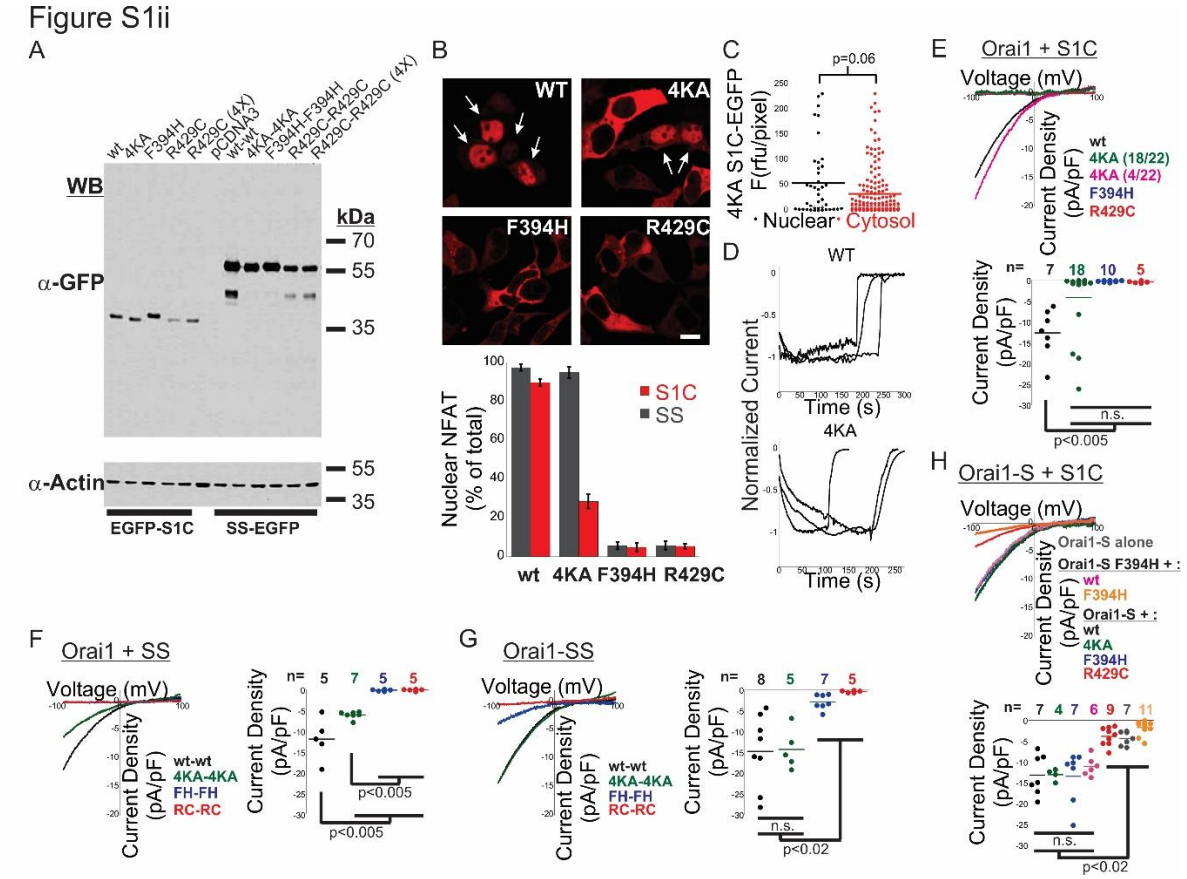

Figure S1ii: Expression and functional analysis of S1C and SS constructs, Related to Figure 1. (A) Western blot analysis of cell lysate prepared from cells expressing the indicated EGFP-S1C or SS-EGFP constructs. Anti-GFP and anti-Actin antibodies were used for protein detection. Note the significant increase in SS-EGFP expression compared to EGFP-S1C. To increase expression levels of EGFP-S1C R429C the EGFP-S1C R429C plasmid used for transfection was increased by four fold (4X). (B-Top panel) Representative fluorescent images of NFAT-mCherry in cells co-expressing NFAT-mCherry together with the indicated EGFP-S1C construct. Arrows indicate cells with nuclear localization of NFAT. Scale bar= 10μm (B- Lower panel) Quantification of nuclear localization of NFAT in HEK293 cells transfected with the indicated SS-EGFP (wt n=92, 4KA n=121, F394H n=80 and R429C n=162) or EGFP-S1C (wt S1C n=149, 4KA S1C n=212, F394H S1C n=167 and R429C S1C n=247) constructs together with Orai1-HA. Note that in the vast majority of cells expressing high levels of SS-EGFP 4KA, NFAT localizes predominantly to the nucleus (in 95±2.9 % of cells) but in cells expressing lower levels of S1C-EGFP 4KA, nuclear localization of NFAT is seen in a smaller population of cells (in 28.5±3.6 % of cells). (C) Distribution of S1C-EGFP (4K/A) fluorescence from cells with nuclear (n=32) or cytosolic (n=110) localization of NFAT. Note that expression levels of S1C 4KA in cells exhibiting nuclear localization of NFAT is slightly higher than in cells with cytosolic localization of NFAT, however, this difference does not reach statistical significance. (D) Time course of current development from three individual cells co-expressing Orai1-EGFP together with mCherry-S1C (left) or mCherry-S1C 4KA (right). Recordings in each group start within a few seconds after cell break-in and 50μM La^{3+} was applied after maximal current magnitude was stabilized. (E) Plots of current-voltage (IV) relationship (Top panel) and distribution of current densities (Lower panel) of currents recorded from a cells expressing Orai1-EGFP together with the indicated mCherrsy-S1C construct. Note the atypical IV curves form cells co-expressing Orai1-EGFP and mCherry-S1C 4KA. Representative trace from responding cells (4 cells out of 18 exhibited similar currents) is shown in pink and a representative trace from non-responding (green trace, 18 cells out of 22 exhibited similar currents) in green. (F) Plots of current-voltage (IV) relationship (Top panel) and distribution of current densities (Lower panel) recorded from a cells expressing mCherry-Orai1 together with the indicated SS-EGFP construct. (G) Distribution of IV plots (Top panel) and current densities (Lower panel) of currents recorded from cells expressing the indicated Orai1-SS-EGFP constructs (G) or from cells co-expressing Orai1-S-EGFP together with the indicated mCherry-S1C constructs (H).

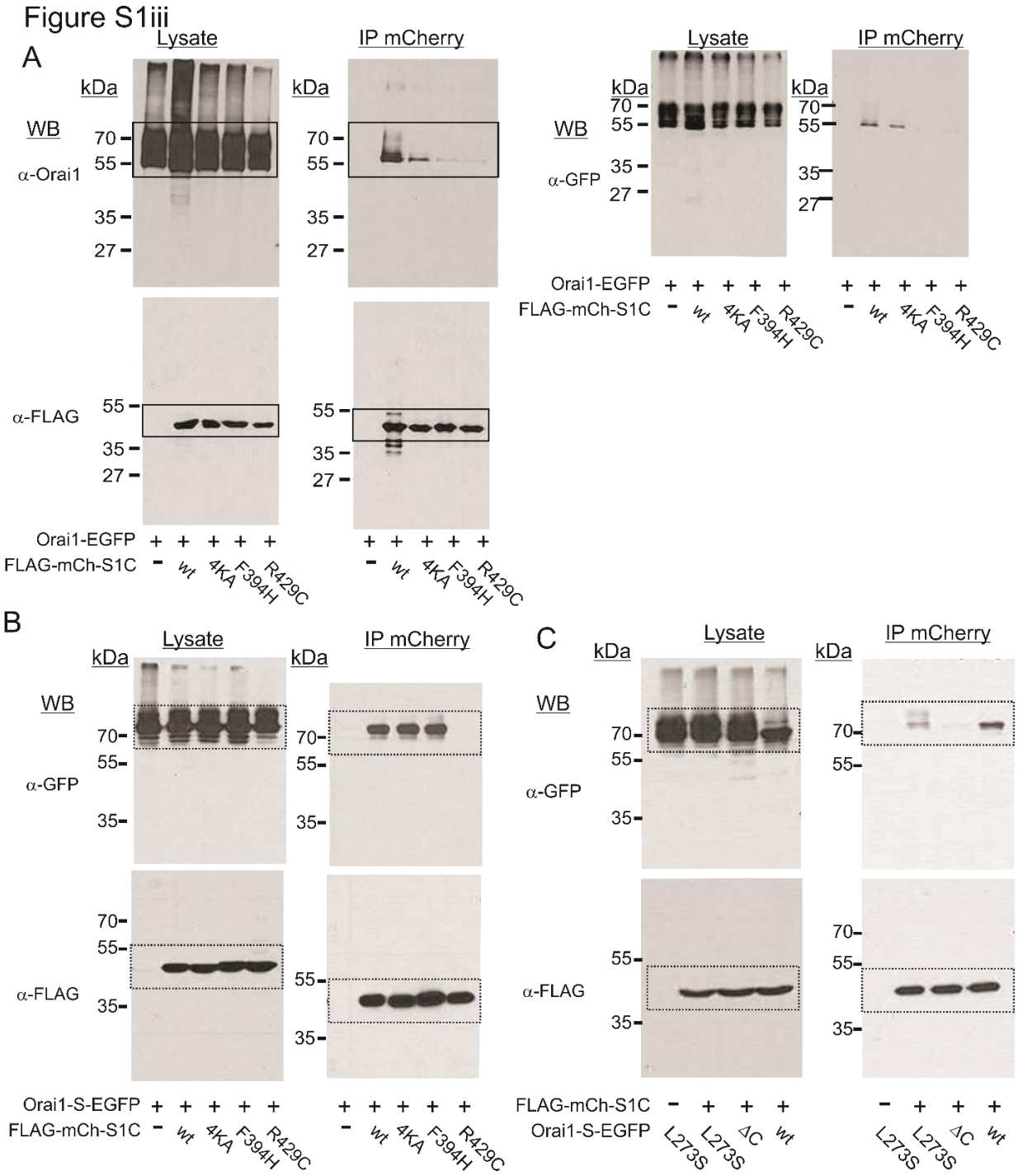

Figure S1iii: Full western-blot images, Related in Figure 1. Rectangles indicate the truncated area used in Figure 1.

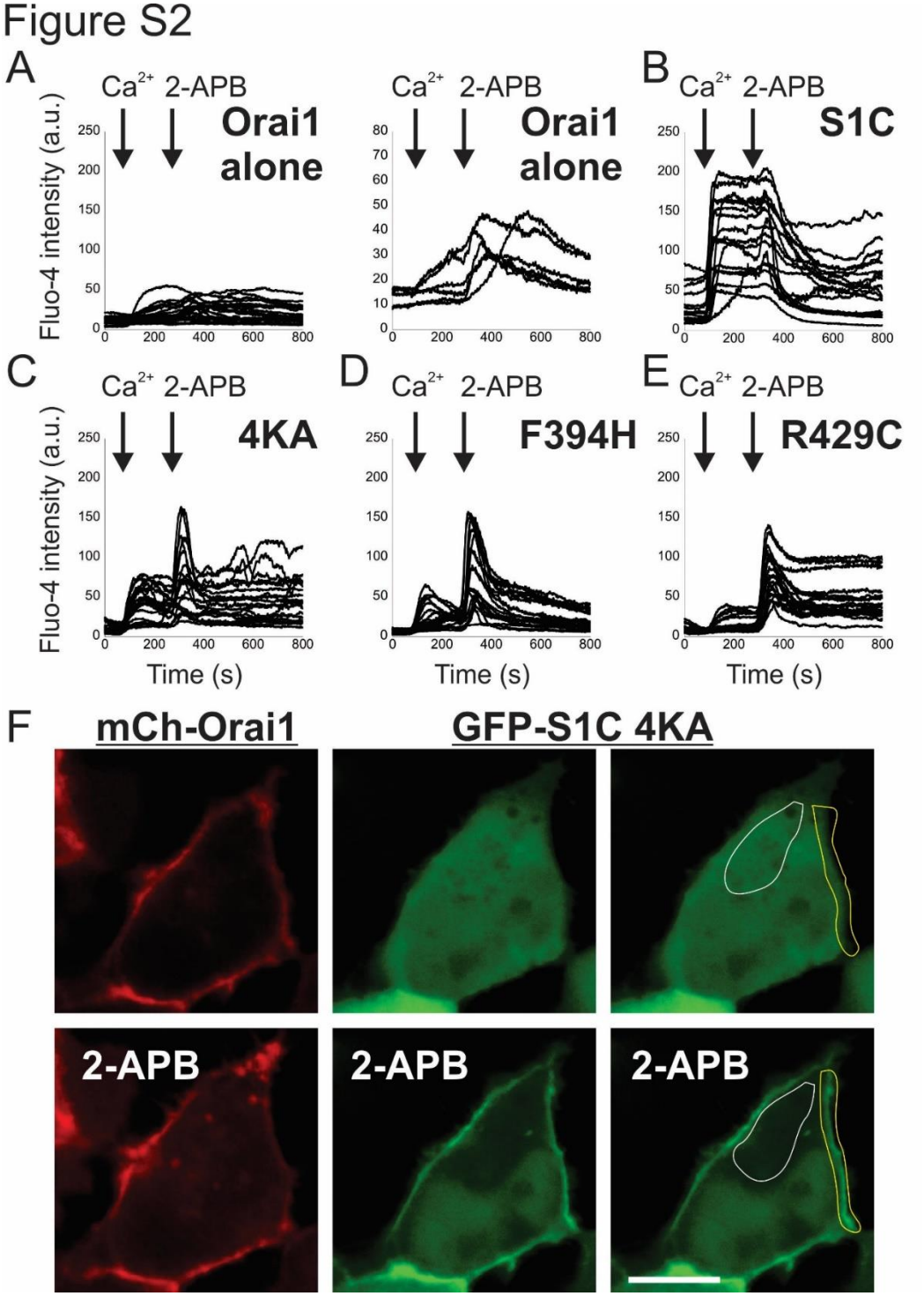

Figure S2: Supporting information, Related to Figure 2. (A-E) Intracellular Ca^{2+} traces recorded from individual HEK293 cells expressing Orai1 alone (A, n=20) or together with the indicated mCherry-S1C construct (B-E, n=17-25 cells in each). Arrows specify time points when 2mM Ca^{2+} and 50μM 2-APB were added to the extracellular solution. Note that a different fluorescence intensity scale is shown for right panel in (A). (F) Method for calculating the ratio of EGFP–S1C intensity at the plasma membrane (PM) compared to the cytosol (Cyto). PM (yellow) and cytosolic (white) regions were determined based on mCherry-Orai1 fluorescence and subsequently used to estimate the mean fluorescence of GFP-S1C in each cellular compartment. Scale bar= 10μm

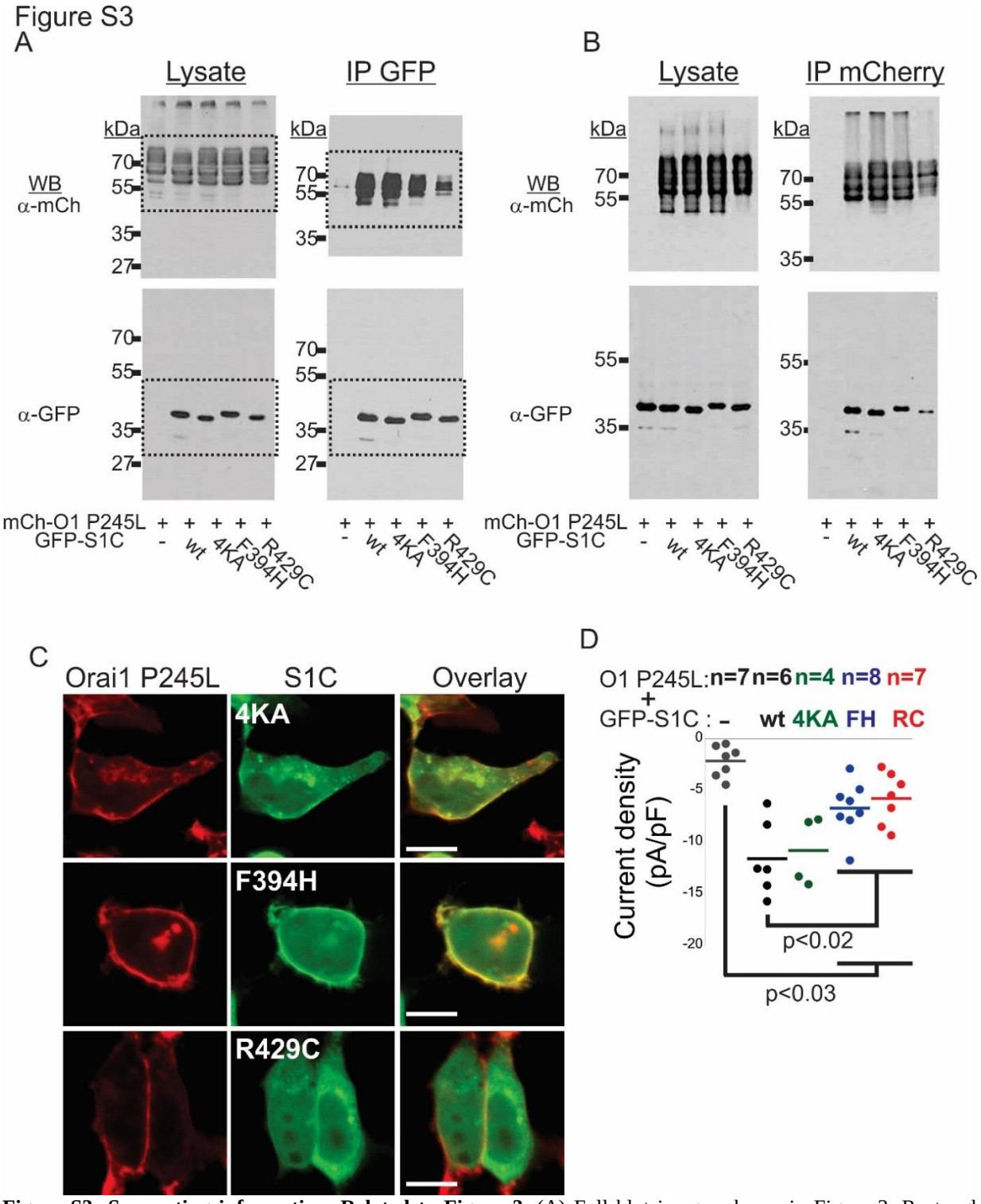

Figure S3: Supporting information, Related to Figure 3. (A) Full blot images shown in Figure 3. Rectangles indicate the truncated area used in Figure 3. (B) Western blot analysis of cell lysate or IP material prepared from cells expressing the indicated EGFP-S1C constructs together with mCherry-Orai1 P245L. Agarose beads conjugated to anti-mCherry nanobodies were used to immunoprecipitate mcherry tagged Orai1 P245L proteins and antibodies against GFP and mCherry were used for protein detection. (C) Representative fluorescent images of the indicated EGFP-S1C mutants and mCherry-Orai1 P245L. Scale bar= 10μm (D) Distribution of current densities recorded from cells co-expressing mCherry-Orai1 P245L alone or together with the indicated EGFP-S1C constructs.

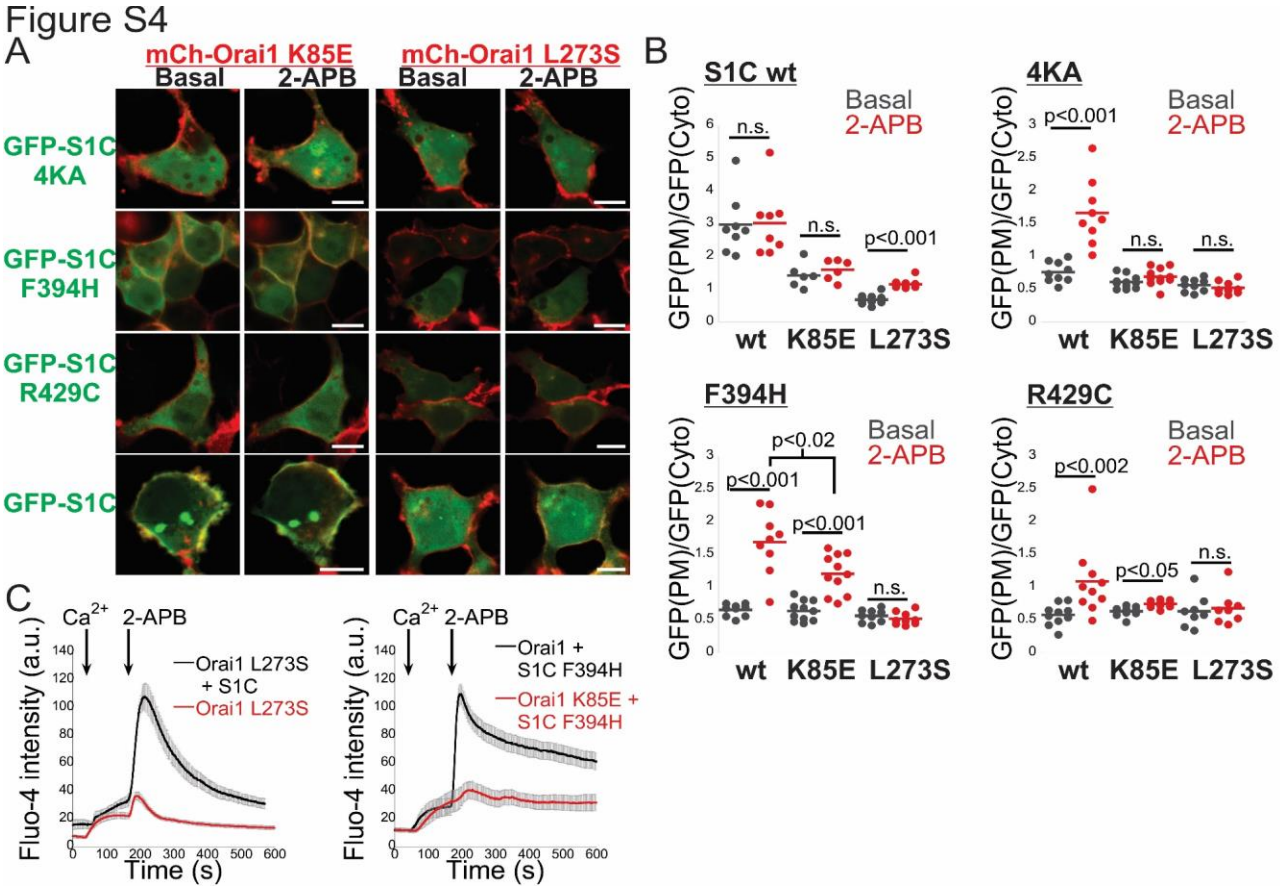

Figure S4: Supporting information, Related to Figure 4. (A) Representative fluorescent images of the indicated EGFP-S1C mutants expressed together with the indicated mCherry-Orai1 construct before and after application of 2-APB (50μM). Scale bar= 10μm (B) The distribution of ratio values of EGFP–S1C fluorescence at the plasma membrane normalized to that in the cytosol measured from cells expressing the indicated S1C and Orai1 constructs. (C) Averaged intracellular Ca^{2+} responses in cells expressing (Left) the Orai1 L273S alone (n=40) or together with S1C (wt n=27) or in cells expressing (Right) S1C F394H together with wt Orai1 (n=32) or with Orai1 K85E (n=21) following addition of Ca^{2+} (2mM) and 2-APB (50μM) to the extracellular solution as marked by arrows.

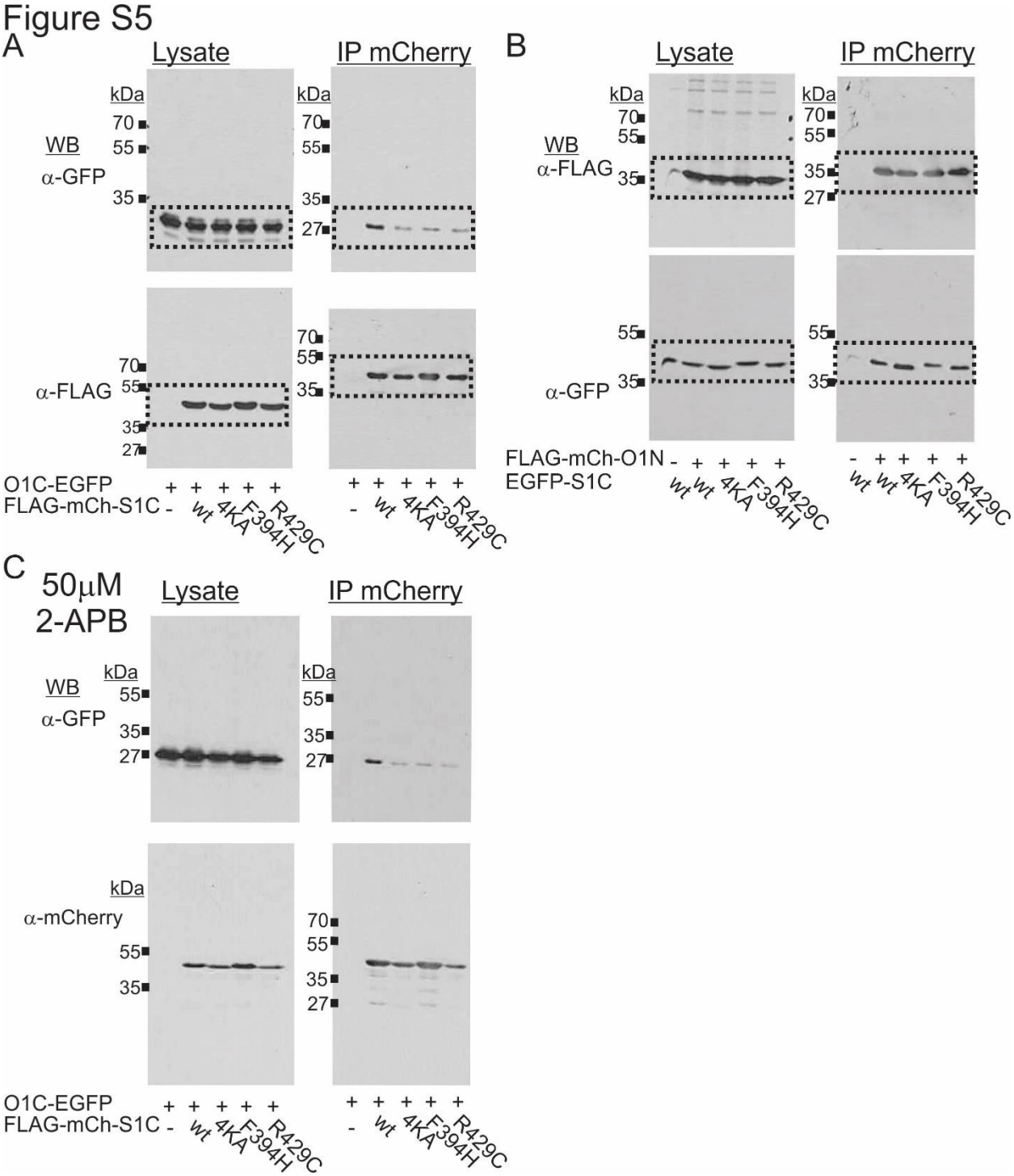

Figure S5: Supporting information, Related to Figure 5. (A-B) Full western-blot images shown in Figure 5. Rectangles indicate the truncated area used in Figure 5. (C) Western blot analysis of cell lysate or immunoprecipitated material (IP) prepared from cells expressing the indicated FLAG-mCherry-S1C constructs together with EGFP tagged Orai1 C terminal fragment (residues 264-301) and treated with 50μM 2-APB for 30 minutes.

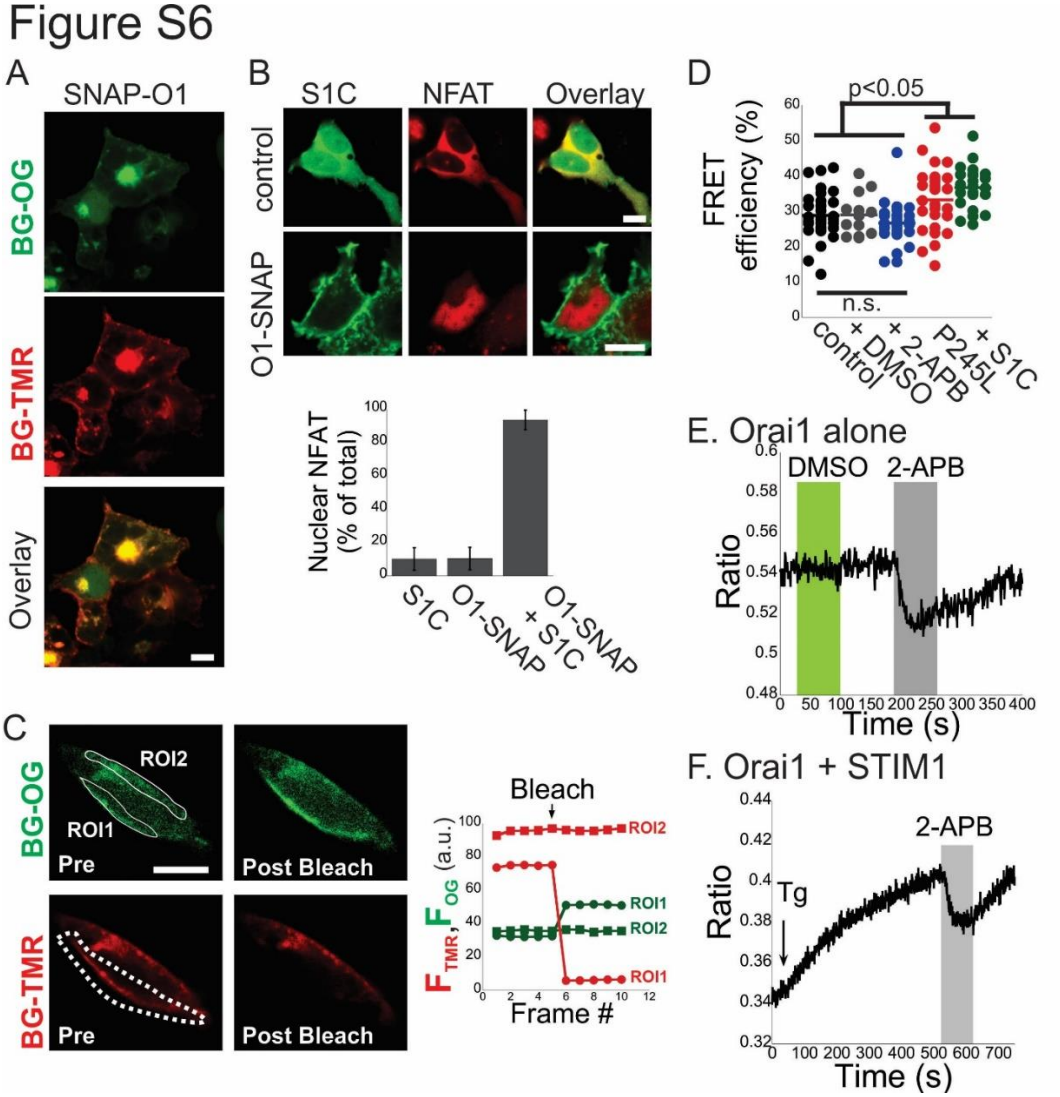

Figure S6: Supporting information, Related to Figure 6. (A) Representative fluorescent images of cells expressing SNAP-Orai1 and labeled with BG-Oregon-Green (OG) and BG-TMR. (B-Top panel) Representative images of NFAT-mCherry and EGFP-S1C fluorescence captured in cells co-expressing these constructs alone or together with Orai1-SNAP. Note that S1C and NFAT localize to the cytosol when expressed alone, but when co-expressed with Orai1-SNAP, S1C localizes to plasma membrane and NFAT to nucleus. (B- Lower panel) Quantification of nuclear localization of NFAT (n=31-56 cells) in HEK293 cells transfected with the indicated combination of S1C and Orai1-SNAP constructs. Scale bar= 10μm (C-Left) Images of BG-OG or BG-TMR fluorescence recorded from a cell expressing Orai1-SNAP and co-labeled with BG-OG and BG-TMR before and after 560nm bleaching illumination of the indicated area in white. (C-Right) Time course of fluorescence intensity of BG-OG and BG-TMR recorded from two regions of interest (ROI1 and ROI2, see inset on Right) in a cell expressing Orai1-SNAP and co-labeled with both fluorophores. In ROI1 but not in ROI2, at the indicated time point BG-TMR fluorescence is bleached with prolonged high intensity 560nm laser. Note that following the 560nm bleach step TMR fluorescence is diminished while OG fluorescence increases in ROI1 while fluorescence of either fluorophores is unchanged in ROI2. Scale bar= 10μm (D) Distribution of FRET efficiencies between BG-OG and BG-TMR recorded in labeled cells expressing Orai1-SNAP P245L, Orai1-SNAP alone (control) or together with S1C, and subjected to treatment with DMSO or 2-APB, as indicated. (E) Time course of averaged donor and acceptor ratios in a cell expressing Orai1-SNAP alone following consecutive treatments with vehicle (DMSO, green background) and 2-APB (grey background), as indicated. (E) Time course of averaged donor and acceptor ratios in cells expressing (n=9) Orai1-SNAP together with STIM1 following consecutive treatments with Tg (1μM, arrow) and 2-APB (50 μM, grey background), as indicated.